

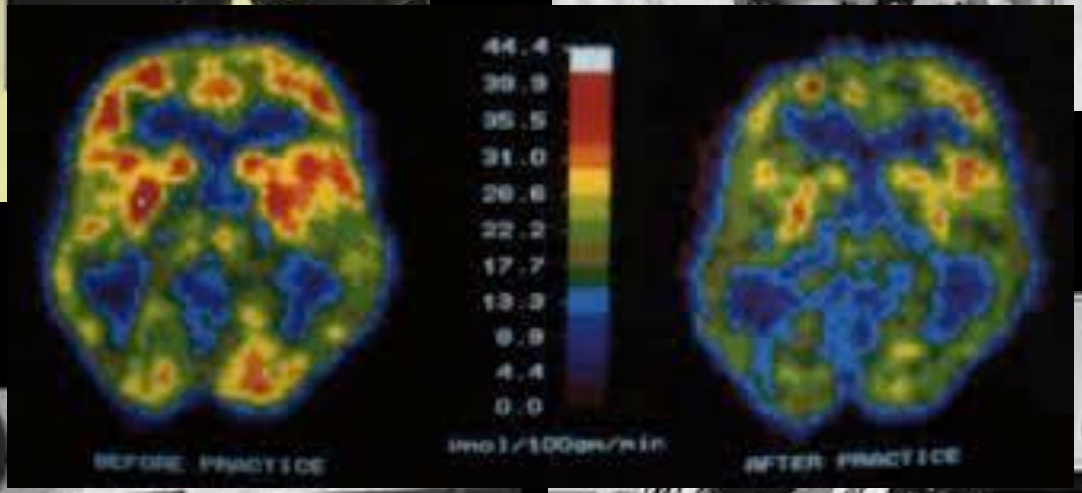
NOS PREMIERS PAS EN NEUROLOGIE NUCLEAIRE

Docteur Mehdi KRIM
Cabinet d'imagerie scintigraphique
Sidi Bel Abbes













UN PEU D'HISTOIRE

Histoire





1957 Travaux de Ter Bogossian avec l'$^{15}O2$ inhalé

1967 Images pas belles

Jusqu'en 1985

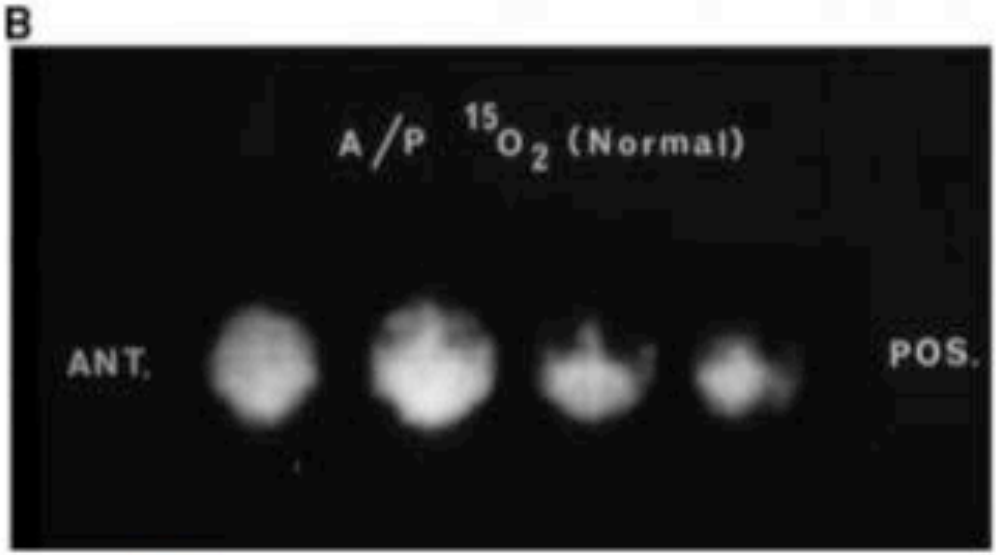
Des travaux n'ayant abouti qu'en 1985 avec

-Images de perfusion

-Images de consommation locale d'O2 en mL/mL sg/min

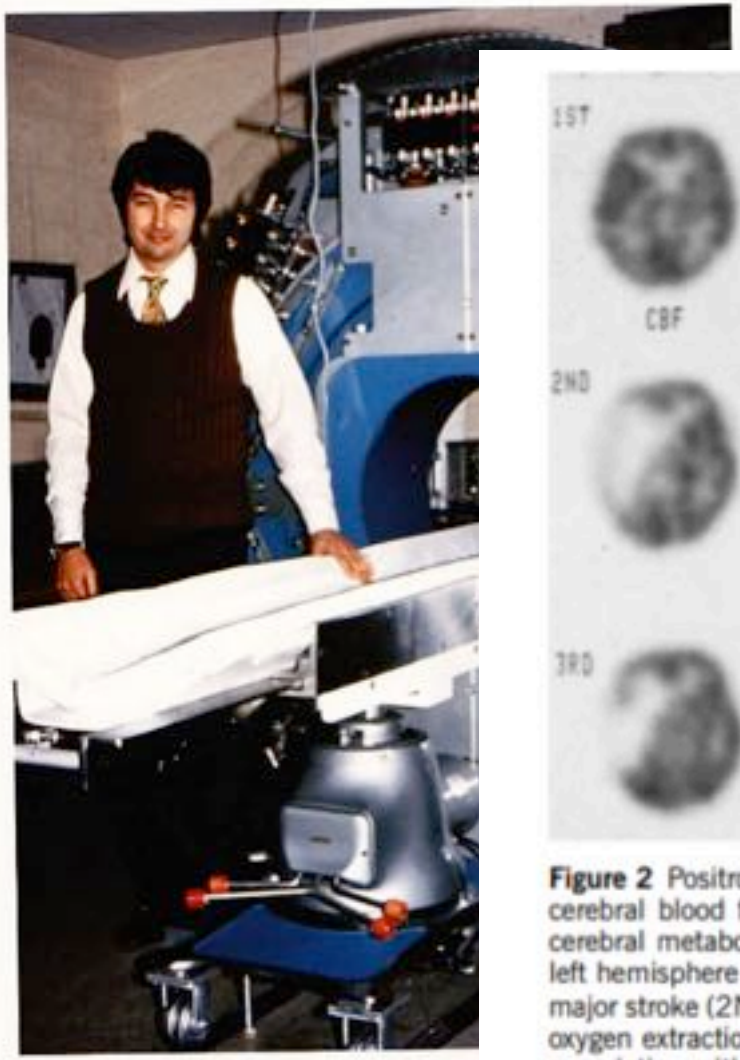
- 1973, 1976 travaux de Jones
  - Perfusion cérébrale à l'équilibre
- Dans les années 1970 avec Anger Cameras avec $^{15}O2$
  - Stroke (Lenzi 1978)
  - Tumeurs cérébrales (McKenzie 1978)
  - Lupus (Pinching 1978)
  - Parkinson D (Lenzi 1979)
- 1974 Equipe d'Orsay: pharmacocinétique de différentes drogues psychotropes marquée au ^{11}C





The development, past achievements, and future directions of brain PET

Terry Jones[1] and Eugenii A Rabiner[2]



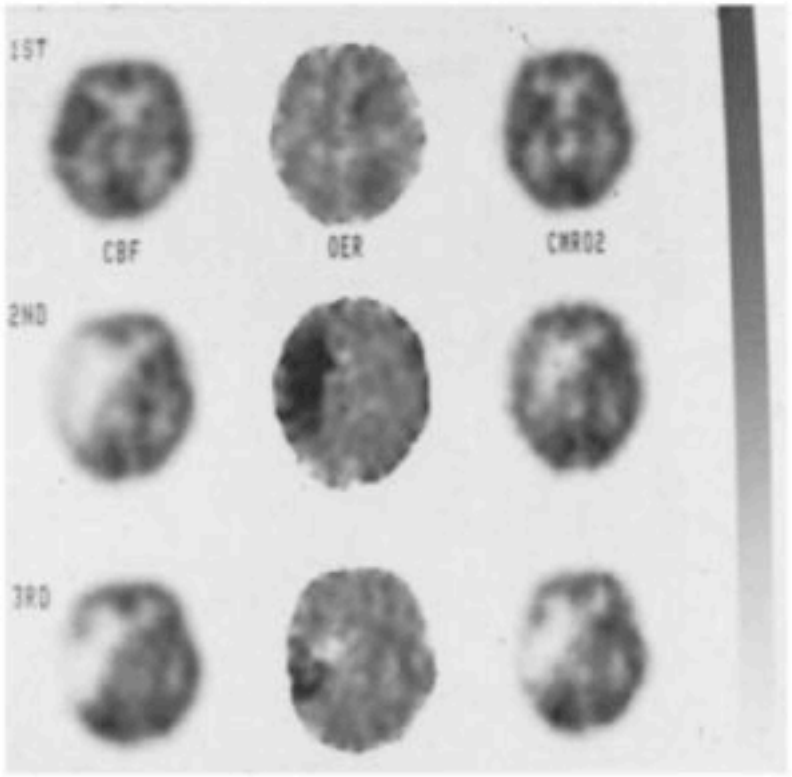
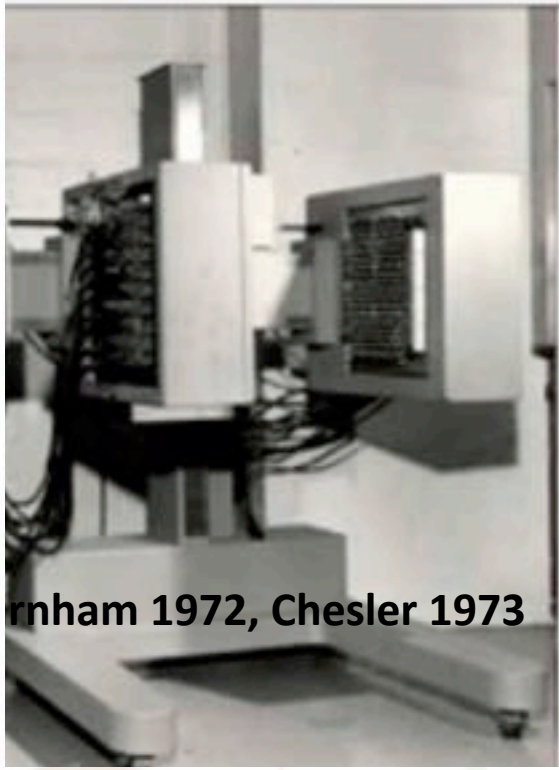


Figure 2 Positron emission tomography (PET) images depicting cerebral blood flow (CBF), oxygen extraction ratio (OER), and cerebral metabolic rate of oxygen ($CMRO_2$) of a patient after a left hemisphere transient ischemic attack (1ST), 7 hours after a major stroke (2ND), and 4 days after the stroke (3RD). The high oxygen extraction ratio seen within hours after the stroke fell in association with a decline in cortical oxygen metabolism (Wise *et al*, 1983).



rnham 1972, Chesler 1973

Nuclear Medicine Communications **6**, 443–447 (1985)

Cerebral uptake and retention of $^{99}Tc^{m}$-hexamethylpropyleneamine oxime ($^{99}Tc^{m}$-HM-PAO)

R.A. HOLMES, S.B. CHAPLIN, K.G. ROYSTON, T.J. HOFFMAN and W.A. VOLKERT

Nuclear Medicine and Research Services Harry S. Truman Memorial Veterans Hospital and Department of Radiology, University of Missouri Health Sciences Center, Columbia, Missouri, USA

D.P. NOWOTNIK, L.R. CANNING, S.A. CUMMING, R.C. HARRISON, B. HIGLEY, G. NECHVATAL, R.D. PICKETT, I.M. PIPER and R.D. NEIRINCKX

Amersham International plc, Amersham, Buckinghamshire, UK

Received 28 May 1985

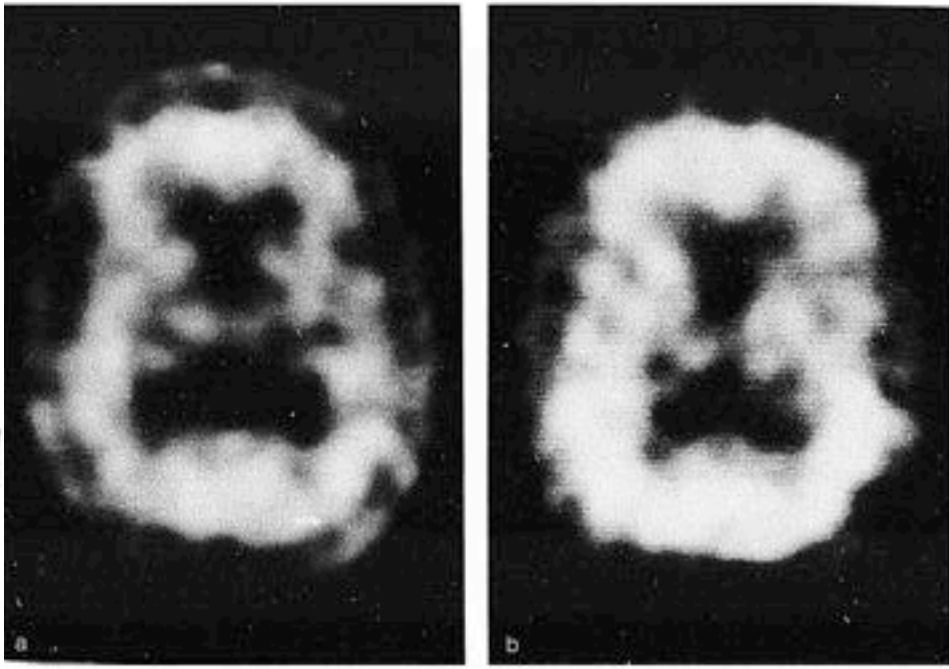


Fig. 2. Transverse SPECT images of $^{99m}Tc^{m}$-HM-PAO in normal volunteer at (a) 5 min and (b) 2 h post injection.

The behavior of ^{99m}Tc-hexamethylpropyleneamineoxime (^{99m}Tc-HMPAO) in blood and brain

Kayoko Nakamura[1], Yasusi Tukatani[1], Atsushi Kubo[1], Shozo Hashimoto[1], Yasuo Terayama[2], Takahiro Amano[2], and Fumio Goto[2]

[1] Department of Radiology, [2] Department of Internal Medicine, School of Medicine, Keio University, Shinjuku-ku, Tokyo 160, Japan

Eur J Nucl Med (1989) 15:100–107

anmnl
Association Nationale de Médecine Nucléaire Libérale

Imagerie de la neurotrasmission

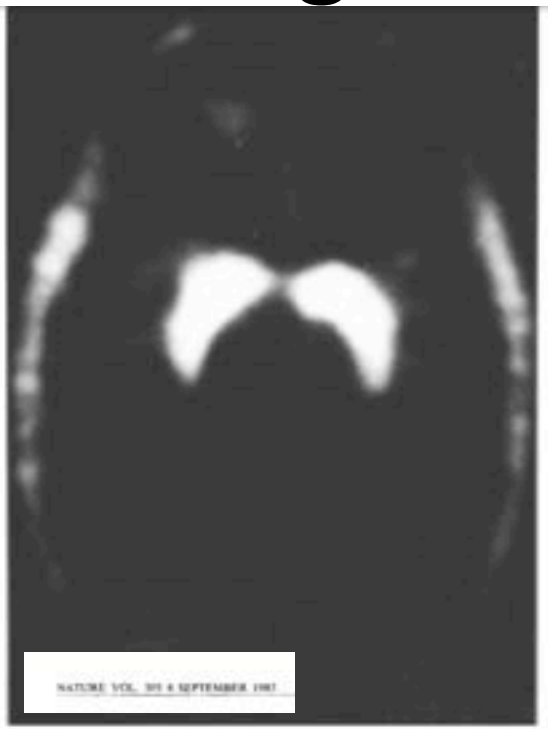


Fig. 1 Tomographic section, face uppermost, obtained in man 3 h after the intravenous injection of ^{18}F-6-fluoro-L-dopa. The section was taken parallel to and 3 cm above the orbito-meatal line. It shows specific accumulations of ^{18}F (white) in the striatum and to a lesser degree in the anterior cingulate and frontal cortex. The accumulation of ^{18}F in the perimeter is due to scalp.

Dopamine visualized in the basal ganglia of living man

E. S. Garnett, G. Firnau & C. Nahmias

Department of Nuclear Medicine, McMaster University Medical Centre, 1200 Main Street West, Hamilton, Ontario, Canada L8N 3Z5

RESEARCH ARTICLE

23 June 1983; revised 8 August 1983

SCIENCE, VOL. 221

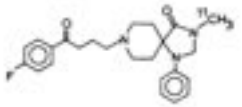
Imaging Dopamine Receptors in the Human Brain by Positron Tomography

Henry N. Wagner, Jr., H. Donald Burns, Robert F. Dannals
Dean F. Wong, Bengt Langstrom, Timothy Duelfer, J. James Frost
Hayden T. Ravert, Jonathan M. Links, Shelley B. Rosenbloom
Scott E. Lukas, Alfred V. Kramer, Michael J. Kuhar

One of the most intriguing problems in biomedical research today is that of re- as a result of neuroleptic therapy (4). The development of positron emission

cose, [^{11}C]carboxyhemoglobin, ionic rubidium-82, ^{68}Ga-labeled EDTA, and other radiopharmaceuticals, and subsequent imaging of the distribution of the radioactive label in the brain by means of the tomographic method, based on detection of the annihilation radiation produced during positron emission (9).

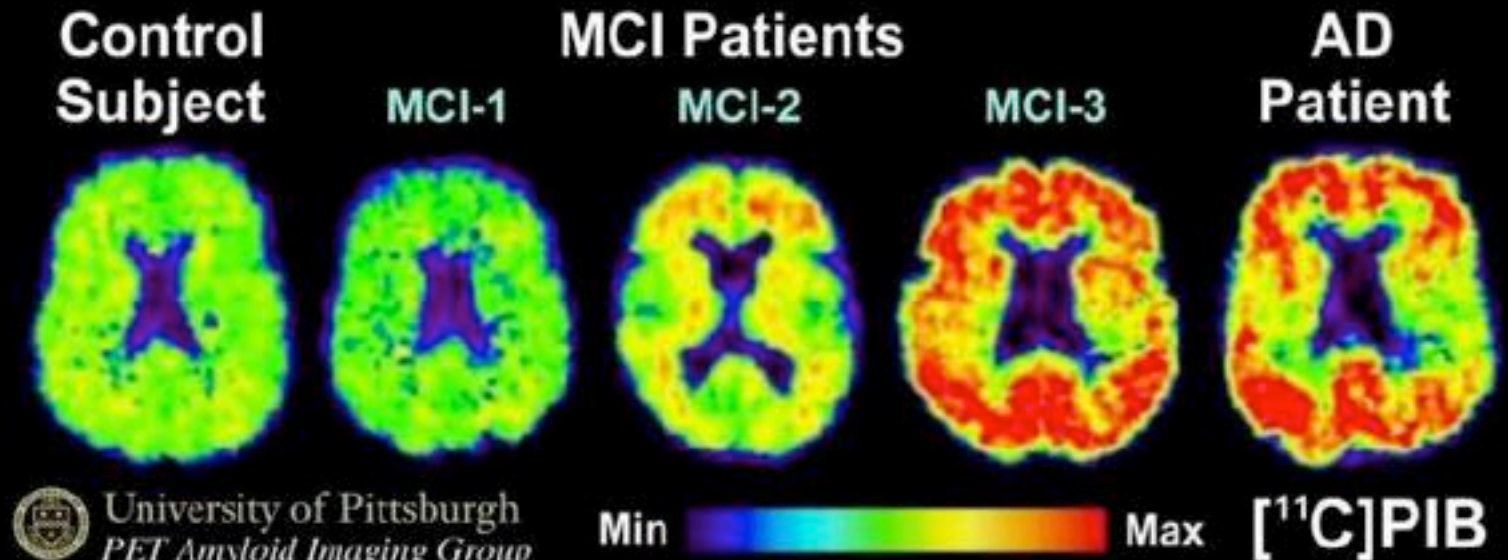
The butyrophenone neuroleptic drug spiperone has been useful in binding studies for measuring dopamine rec tors both in vitro (10) and in vivo (1 We now report initial results obtained with 3-*N*-[^{11}C]methylspiperone (^{11}C-NMSP), a spiperone derivative, in



Neurotransmission	*AAAD*	[^{18}F]FDOPA	
	Dopamine	[^{11}C]SCH-23390	
	D_1 receptors	[^{11}C]NNC-112	
	Dopamine	[^{11}C]Raclopride	[^{123}I]IBZM
	D_2 receptors	[^{18}F]Fallypride	
	Dopamine transporters (DT)	[^{11}C]Cocaine	^{123}I-β-CIT
		[^{18}F]FP-CIT	^{123}I-Altropane
		[^{18}F]FE-CNT	^{99m}Tc-TRODAT1
	Vesicular amine transporter (VMAT)	[^{11}C]DTBZ	
		[^{18}F]DTBZ	
	5-HT_{1A} receptor	[^{11}C]DWAY	
		[^{18}F]MPPF	
	5-HT_{2A} receptor	[^{18}F]Altanserin	
		[^{18}F]Setoperone	
	5-HT transporter	[^{11}C](+)McN-5652	^{123}I-IDAM
		[^{11}C]DASP	
	mACh receptor	[^{18}F]FP-TZTP	
	nACh receptor	[^{18}F]NFEP	
		[^{11}C]PMP and AMP	
	μ-Opiate receptor	[^{11}C]Carfentanil	
	GABA receptor	[^{18}F]Flumazenil	^{123}I-Iomazenil
		[^{11}C]Flumazenil	

Molecular imaging
Shankar Vallabhajossula
© Springer-Verlag Berlin Heidelberg 2009

PIB in Controls, MCI, AD

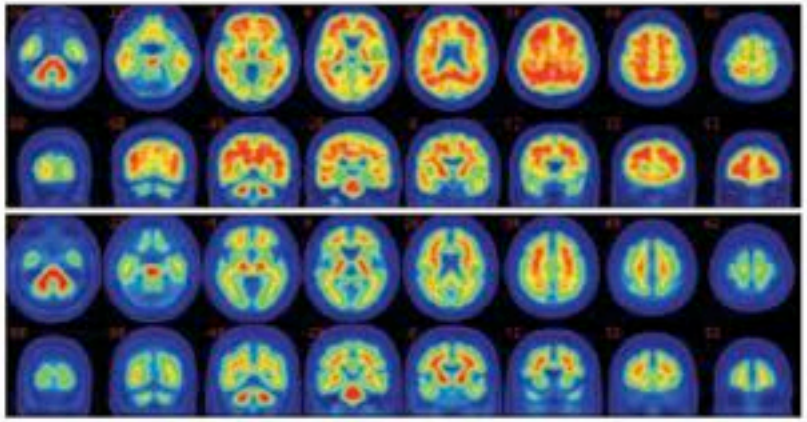


Some MCI's have control-like PIB levels, some have AD-like levels, and some have intermediate levels

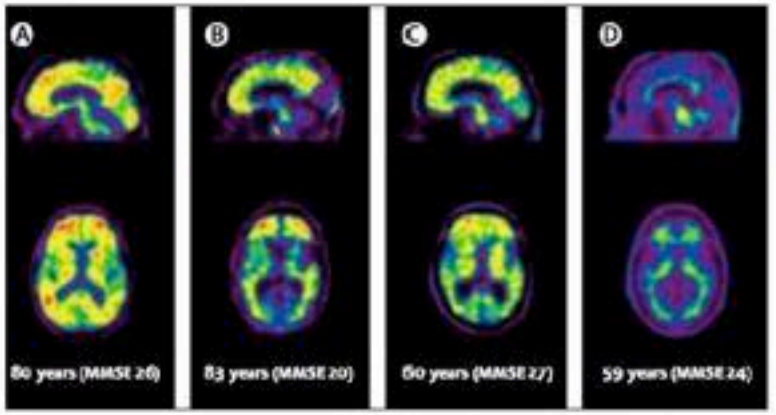
Price et al., JCBFM 25:1528 (2005)
Lopresti et al., J Nucl Med 46:1959 (2005)

2013-2014

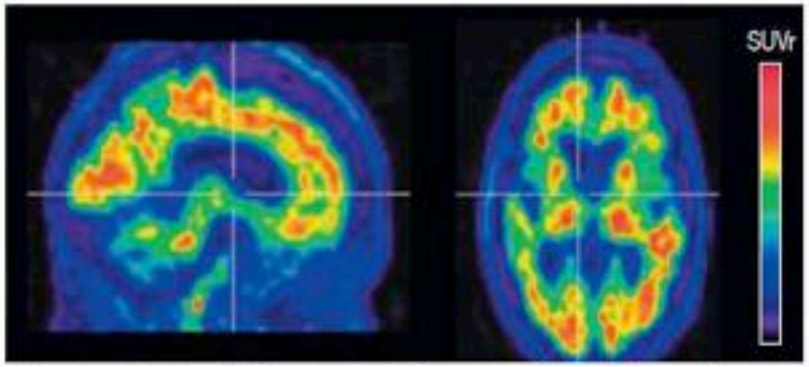
• **^{18}F-PIB Flutemetamol** (GE Healthcare)



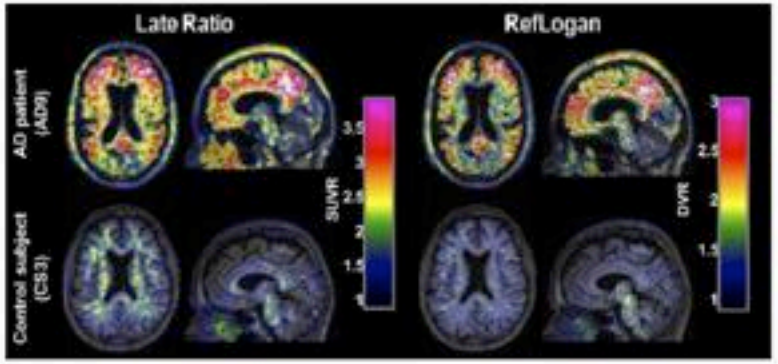
• **AV1 ou ^{18}F-BAY94 Florbetaben** (Bayer/Piramal)



• **AV 45 ou Florbetapir** (Amyvid, Lilly/Avid)



•**AZD 4694 NAV4694** (Navidea/Astra Zeneca)



Clark CM et al. Use of Florbetapir-Pet for imaging ß-amyloid pathology. JAMA 2011.
Rowe CC et al. Imaging of amyloid beta in Alzheimer's disease with 18F-BAY94-9172, a novel PET tracer: proof of mechanism. Lancet Neurol 2008.
Vandenberghe R et al. 18F-Flutemetamol Amyloid Imaging in Alzheimer Disease and Mild Cognitive Impairment A Phase 2 Trial. Ann Neurol 2010.
Zsolt Cselényi et al. Clinical Validation of 18 F-AZD4694, an Amyloid- ß–Specific PET Radioligand. JNM 2011.

Plus récemment

Original Article

JCBFM

Journal of Cerebral Blood Flow & Metabolism
0(00) 1–15
© Author(s) 2018
Reprints and permissions:
DOI: 10.1177/0271678X18771242
journals.sagepub.com/home/jcbfm
SAGE

Substitution of venous for arterial blood sampling in the determination of regional rates of cerebral protein synthesis with L-[1-^{11}C]leucine PET: A validation study

Giampaolo Tomasi[1], Mattia Veronese[2], Alessandra Bertoldo[3], Carolyn B Smith[1] and Kathleen C Schmidt[1]

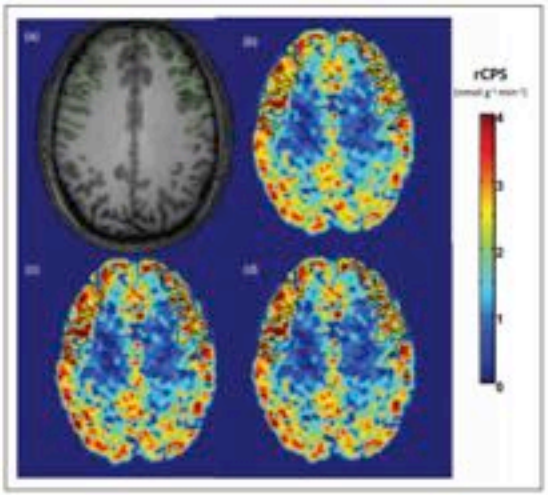


Figure 5. Effects of input function on computed values of rCPS in a healthy 23-year-old male scanned while awake. The injected dose of L-[1-^{11}C]leucine was 25 mCi (0.30 mCi/kg) (a) MRI; (b) rCPS computed with the measured arterial input function; (c) rCPS computed with the venous-calibrated population-derived input function that utilizes 15, 30, 45 and 60 min venous samples for calibration together this subject's measured venous plasma leucine concentration; (d) rCPS computed with the venous-calibrated population-derived input function that utilizes 30, 45 and 60 min venous samples for calibration together this subject's measured venous plasma leucine concentration. Images are in the transverse plane and the frontal cortex is outlined. Images of rCPS computed with the venous-calibrated population-derived input functions (c, d) are almost indistinguishable from the rCPS image determined from the measured arterial input function (b).

JNM The Journal of NUCLEAR MEDICINE

Age-related change in 5-HT6 receptor availability in healthy male volunteers measured with ^{11}C-GSK215083 PET

Rajiv Radhakrishnan, Nabeel Nabulsi, Edward Gaiser, Jean-Dominique Gallezot, Shannan Henry, Beata Planeta, Shu-fei Lin, Jim Ropchan, Wendol Williams, Evan Morris, Deepak Cyril D'Souza, Yiyun Huang, Richard E. Carson and David Matuskey

J Nucl Med.
Published online: April 6, 2018.
Doi: 10.2967/jnumed.117.206516

JNM The Journal of NUCLEAR MEDICINE

Human Kinetic Modeling of the 5HT6 PET Radioligand ^{11}C-GSK215083 and Its Utility for Determining Occupancy at Both 5HT6 and 5HT2A Receptors by SB742457 as a Potential Therapeutic Mechanism of Action in Alzheimer Disease

Christine A. Parker, Eugenii A. Rabiner, Roger N. Gunn, Graham Searle, Laurent Martarello, Robert A. Comley, Maria Davy, Alan A. Wilson, Sylvain Houle, Romina Mizrahi, Marc Laruelle and Vincent J. Cunningham

J Nucl Med. 2015;56:1901-1909.
Published online: September 17, 2015.
Doi: 10.2967/jnumed.115.162743

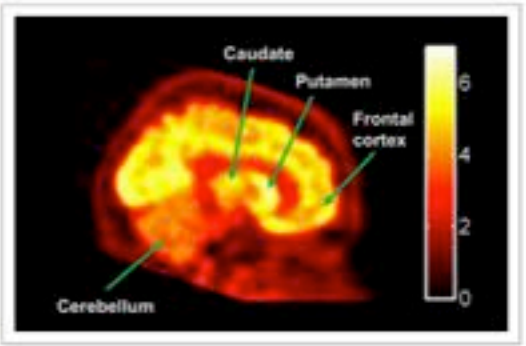


FIGURE 2. Baseline PET image demonstrating heterogeneous biodistribution of ^{11}C-GSK215083 in human brain (scale bar = percentage injected dose per liter).

Imagerie des recepteurs sérotoninergiques

NEWSLINE

Nuclear Medicine Pioneer: Benedict Cassen

The Rectilinear Scanner and an Enduring Legacy of Education and Research





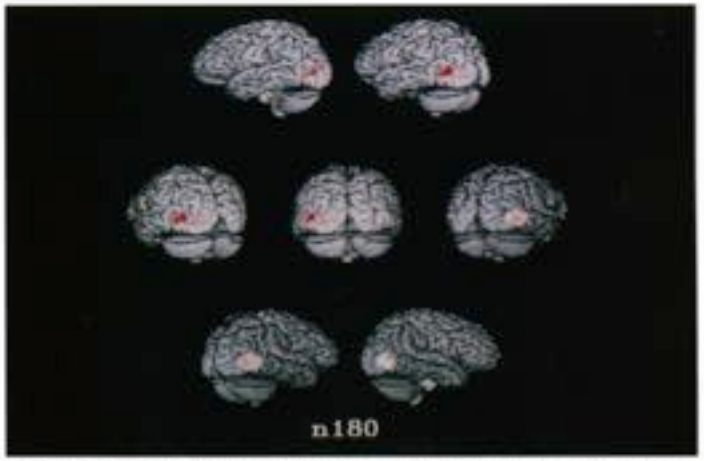
J. Anat. (1994) 184, pp. 211–225, with 10 figures Printed in Great Britain

Review

Functional neuroanatomy of the human brain: positron emission tomography – a new neuroanatomical technique

R. S. J. FRACKOWIAK AND K. J. FRISTON

MRC Cyclotron Unit, Hammersmith Hospital, London, UK



Journal of Cerebral Blood Flow & Metabolism (2012) 00, 1–29

Table 1 Principal radiotracers used for human brain PET studies to date

Radiotracer	*Targets*	*Referenc*
[^{11}C]psychotropic drugs	Drug pharmacokinetics	Raynaud *et al* (1974)
[^{18}F]FDG	Glucose utilization	Kuhl *et al* (1976)
[^{11}C]methionine	Amino-acid transport	Comar *et al* (1976) *Eur J Nucl Med* 1:11–14
[^{11}C]unnatural amino acids	Amino-acid transport	Hubner *et al* (1979) *J Nucl Med* 20:507–513
[^{15}O]oxygen	Oxygen utilization	Frackowiak *et al* (1980)
[^{15}O]water	Blood flow	Frackowiak *et al* (1980)
[^{11}C]leucine	Protein synthesis	Barrio *et al* (1983)
[^{18}F]F-DOPA	Dopamine synthesis	Garnett *et al* (1983)
[^{11}C]methyl-spiperone	Dopamine and serotonin receptors	Wagner *et al* (1983)
[^{11}C]PK-11195	Peripheral benzodiazepine receptors	Camsonne *et al* (1984) *J Labelled Comp Radiopharm* 21:985–991
[^{11}C]BCNU/carmustine	Drug pharmacokinetics	Diksic *et al* (1984)
[^{11}C]diprenorphine	Nonselective opiate receptors	Jones *et al* (1985) *Lancet* 326:665–666
[^{11}C]carfentanil	μ-Opioid receptor	Frost *et al* (1985) *J Comput Assist Tomogr* 9(2):231–236
[^{11}C]flumazenil (FMZ)	Central benzodiazepine receptors	Samson *et al* (1985) *Eur J Pharmacol* 110:247–251
[^{11}C]raclopride	Dopamine type 2 (D_2) receptor	Ehrin *et al* (1985) *Int J Appl Radiat Isot* 36:269–273
[^{11}C]Schering-23390	Dopamine type 1 (D_1) receptor	Halldin *et al* (1986) *Int J Rad Appl Instrum* 37:1039–1043
[^{11}C]nomifensine	Dopamine transporter (DAT)	Aquilonius *et al* (1987) *Acta Neurol Scand* 76:283–287
[^{11}C]deprenyl	Monoamine oxidase type-B (MAO-B)	Fowler *et al* (1987) *Science* 235(4787):481–485
[^{11}C]McNeil 5652	Serotonin transporter (SERT/5-HTT)	Suchiro *et al* (1993) *Life Sci* 53:883–892
[^{11}C]WAY 100635	Serotonin 5-HT1A receptor	Pike *et al* (1994) *Med Chem Res* 5:208–227
[^{11}C]FBL 457	Dopamine ($D_{2/3}$) receptors	Halldin *et al* (1995) *J Nucl Med* 36:1275–1282
[^{11}C]MTBZ	Vesicular monoamine transporter (VMAT2)	Kilbourn *et al* (1995) *Eur J Pharmacol* 278:249–252
L-1-[^{11}C]tyrosine	Brain tumor protein synthesis	Willemsen *et al* (1995)
[^{11}C]MDL 100907	Serotonin 5-HT2A receptor	Lundkvist *et al* (1996) *Life Sci* 58:187–192
[^{11}C]β-CIT-FE	Dopamine transporter (DAT)	Halldin *et al* (1996) *Synapse* 22:386–390
[^{11}C]PMP	Acetylcholinesterase (ACE)	Kilbourn *et al* (1996) *Synapse* 22:123–131
[^{11}C]verapamil	P-glycoprotein (P-gp) substrate	Elsinga *et al* (1996) *J Nucl Med* 37:1571–1575
[^{11}C]MP4A	Acetylcholinesterase (ACE)	Iyo *et al* (1997) *Lancet* 349:1805–1809
[^{11}C]NNC112	Dopamine (D_1) receptor	Halldin *et al* (1998) *J Nucl Med* 37:2061–2068
[^{18}F]A-85380	Nicotinic acetylcholine receptors	Horti *et al* (1998) *Nucl Med Biol* 25:599–603
[^{18}F]fallypride	Dopamine (D_2) receptor	Mukherjee *et al* (1999) *Nucl Med Biol* 26:519–527
[^{11}C]α-methyl-l-tryptophan	Tryptophan activity	Shoaf *et al* (2000) *J Cereb Blood Flow Metab* 20:244–252
[^{11}C]DASB	Serotonin transporter (SERT/5-HTT)	Ginovart *et al* (2001) *J Cereb Blood Flow Metab* 21:1342–1353
[^{11}C]Ro15-4513	GABA-benzodiazepine receptors	Lingford-Hughes *et al* (2002) *J Cereb Blood Flow Metab* 22:878–889
[^{11}C]temazolomide	Temazolomide pharmacokinetics	Saleem *et al* (2003)
[^{18}F]SPA-RQ	Neurokinin-1 receptor	Solin *et al* (2004) *Mol Imaging Biol* 6:373–384
[^{11}C]PIB	β-Amyloid	Klunk *et al* (2004)
[^{18} F]fluoroethyl-L-tyrosine	Brain tumor protein synthesis	Pauleit *et al* (2005)
[^{18}F]fluorothymidine	Brain tumor proliferation	Chen *et al* (2005)
[^{11}C]harmine	Monoamine oxidase type-A (MAO-A)	Ginovart *et al* (2006)
[^{18}F]MK-9470	Cannabinoid receptor type 1 (CBR-1)	Burns *et al* (2007) *PNAS* 104:9800–9805
[^{11}C]methylreboxetine (MRB)	Norepinephrine transporter (NET)	Logan *et al* (2007) *Nucl Med Biol* 34:667–679
[^{11}C]ABP688	Glutamate receptor 5 (mGluR5)	Ametamey *et al* (2007) *J Nucl Med* 48:247–252
[^{11}C]PBR28*	Translocator protein (TSPO)	Imaizumi *et al* (2008) Neuroimage 39:1289–98

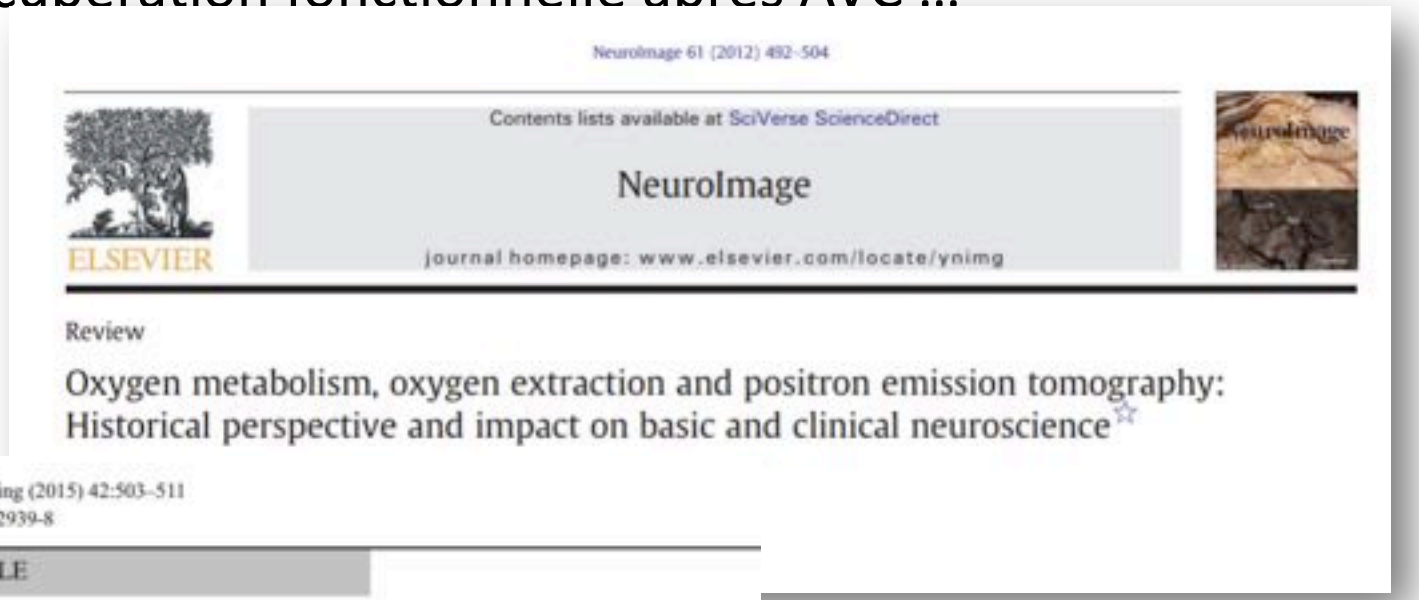
Table 16.2 Radiopharmaceuticals for brain imaging studies

Biological process	Target	Radiopharmaceutical	
		PET	SPECT
Cerebral blood flow		[^{15}O]H_2O	^{99m}Tc-HMPAO (Ceretec™)
			^{99m}Tc-ECD (Neurolite™)
Glucose metabolism	*Hexokinase* and Glucose transporters	[^{18}F]FDG	
Neurotransmission	*AAAD*	[^{18}F]FDOPA	
	Dopamine	[^{11}C]SCH-23390	
	D_1 receptors	[^{11}C]NNC-112	
	Dopamine	[^{11}C]Raclopride	[^{123}I]IBZM
	D_2 receptors	[^{18}F]Fallypride	
	Dopamine transporters (DT)	[^{11}C]Cocaine	^{123}I-β-CIT
		[^{18}F]FP-CIT	^{123}I-Altropane
		[^{18}F]FE-CNT	^{99m}Tc-TRODAT1
	Vesicular amine transporter (VMAT)	[^{11}C]DTBZ	
		[^{18}F]DTBZ	
	5-HT_{1A} receptor	[^{11}C]DWAY	
		[^{18}F]MPPF	
	5-HT_{2A} receptor	[^{18}F]Altanserin	
		[^{18}F]Setoperone	
	5-HT transporter	[^{11}C](+)McN-5652	^{123}I-IDAM
		[^{11}C]DASP	
	mACh receptor	[^{18}F]FP-TZTP	
	nACh receptor	[^{18}F]NFEP	
		[^{11}C]PMP and AMP	
	μ-Opiate receptor	[^{11}C]Carfentanil	
	GABA receptor	[^{18}F]Flumazenil	^{123}I-Iomazenil
		[^{11}C]Flumazenil	
Amyloid plaques	β-Amyloid	[^{18}F]-FDDNP, [^{11}C]PIB	
		[^{18}F]-BAY94–9172	

Molecular imaging
Shankar Vallabhajossula
© Springer-Verlag Berlin Heidelberg 2009

Pathologie vasculaire

- Compréhension des phénomènes physiologiques: l'extraction de l'O2, l'utilisation cérébrale de l'O2, perfusion demisère, penumbra, réserve vasculaire cérébrale, prédiction de la récupération fonctionnelle après AVC …


NeuroImage 61 (2012) 492–504

Contents lists available at SciVerse ScienceDirect

NeuroImage

journal homepage: www.elsevier.com/locate/ynimg

Review

Oxygen metabolism, oxygen extraction and positron emission tomography: Historical perspective and impact on basic and clinical neuroscience☆

Eur J Nucl Med Mol Imaging (2015) 42:503–511
DOI 10.1007/s00259-014-2939-8

ORIGINAL ARTICLE

^{18}F-GE-180: a novel TSPO radiotracer compared to ^{11}C-R-PK11195 in a preclinical model of stroke

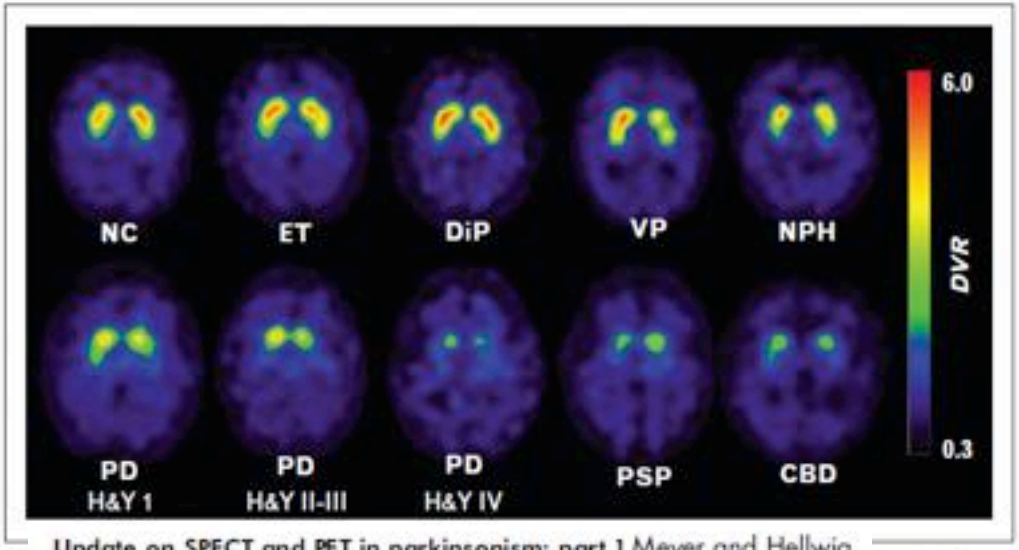
Hervé Boutin · Katie Murray · Jesus Pradillo · Renaud Maroy · Alison Smigova · Alexander Gerhard · Paul A. Jones · William Trigg

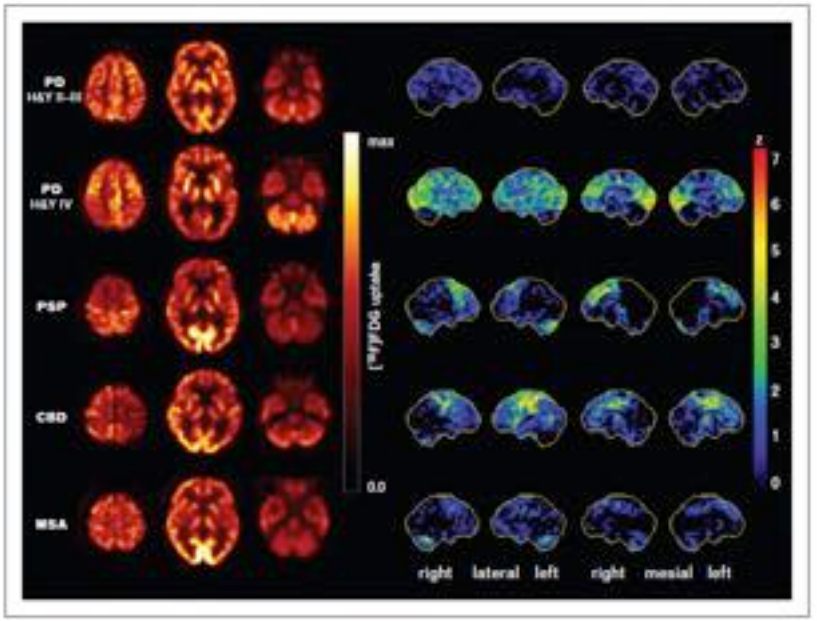
Imaging Microglial Activation with TSPO PET: Lighting Up Neurologic Diseases?

Lucy Vivash and Terence J. O'Brien

J Nucl Med 2016 57 8A

Troubles du mouvement





Update on SPECT and PET in parkinsonism: part 1 Meyer and Hellwig

Curr Opin Neurol 2014, 27:390–397
DOI:10.1097/WCO.0000000000000106

Table 1 Typical Characteristics of Extrapyramidal neurodegenerative Disorders

	Clinical Features				Clinical Imaging		Protein Depositions		
	Bradykinesia/ Rigidity	Postural Instability	Rest Tremor	Other	[18]FIFDG	Striatal [123]I Ioflupane Defects	αSyn	tau	Aβ-Amyloid
PD	Asymmetric limbs	Advanced stages	Common		↑ Striatum (early stages) ↓ Parietal and occipital cortices (later stages)	Asymmetric, putamen > caudate	Lewy bodies, Lewy neurites	Absent	Uncommon
PSP	Axial	Onset	Uncommon	Supranuclear ocular palsy	↓ Striatum ↓ Dorsal & Mesial Frontal Cortices	Symmetric	Absent	4R SF/TF	Uncommon
MSAp	Symmetric Limbs	Advanced stages	Variable	Autonomic failure	↓ Striatum ↓ Cerebellum and pons (variable)	Symmetric	Astrocytes	Absent	Uncommon
CBD	Asymmetric limbs	Uncommon	Uncommon	Dystonia, myoclonus, alien limb	↓ Precentral and postcentral cortex ↓ Striatum ↓ Thalamus	Asymmetric	Absent	4R SF/TF	Uncommon
LBD	Symmetric limbs (variable)	Variable	Uncommon	Visual illusions, cognitive fluctuation	↓ Parietotemporal association cortex ↓ Precuneus cortex ↓ Occipital cortex (variable)	Symmetric	Lewy bodies, Lewy neurites	Variable 3R/ 4R NFT	Frequent

3R, 3-repeat tau isoform; 4R, 4-repeat tau isoform; αSyn, α-synuclein; MSAp, MSA, parkinsonian variant; SF, straight filaments; TF, twisted filaments.

Molecular Imaging of Extrapyramidal Movement Disorders

[illegible] 2010;00:1–7
0031-3998/$ 2010 Elsevier Inc. All rights reserved.

Kirk A. Frey, MD, PhD

Epilepsie

Seizure (2007) 16, 509–520

The contribution of 18F-FDG PET in preoperative epilepsy surgery evaluation for patients with temporal lobe epilepsy
A meta-analysis

O. Willmann [a,b,c], R. Wennberg [b], T. May [c], F.G. Woermann [c], B. Pohlmann-Eden [a,b,c,*]

In conclusion, ipsilateral PET hypometabolism showed high concordance and high predictive values for good outcome, even in cases requiring DEEG with normal MRI or with non-localizing ictal scalp EEG. Our data confirm that ipsilateral PET hypometabolism may be an indicator for good postoperative outcome in the presurgical evaluation of drug-resistant temporal lobe epilepsy, although under cost-effectiveness aspects the role and value remain questionable and unclear. PET does not appear necessary in patients localized by ictal scalp EEG and MRI. Larger prospective multicenter studies with a specific question, e.g. the utility of PET in patients with non-localizing ictal scalp EEG and/or MRI should be obtained.

^{18}F-fluorodeoxyglucose and ^{18}F-flumazenil positron emission tomography in patients with refractory epilepsy

Radiol Oncol 2016; 50(3): 247-253.

Marina Hodolic[1,2], Raffi Topakian[3], Robert Pichler[4]

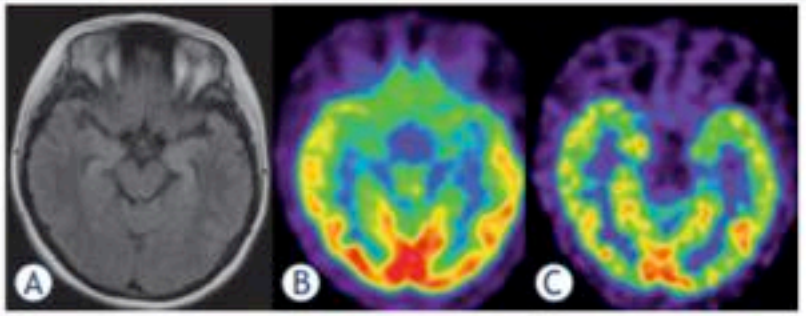


FIGURE 2. ^{18}F-FDG PET (B) scan vs. ^{18}F-Flumazenil PET (C) in a 19 year old female patient with bilateral hippocampal sclerosis as shown by MRI (A). Both PET modalities present low temporomesial uptake being larger on the left side, but benzodiazepine-receptor imaging appears sharper and presents a focal defect.

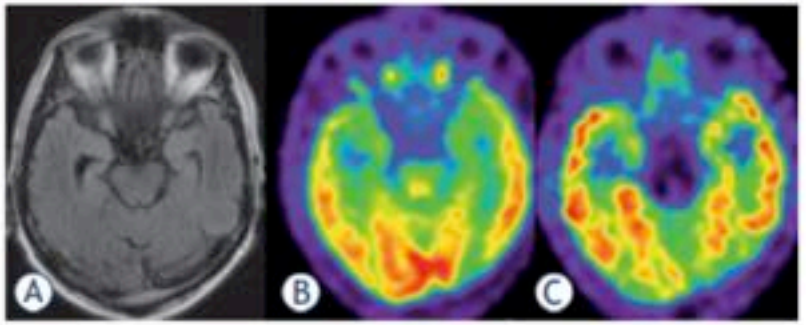


FIGURE 3. Focal epilepsy in 56 year old male patient. (A) MRI: astrogliosis of the right hippocampus (later proven by histology); (B) ^{18}F-FDG PET: minal temporomesial hypometabolism of both sides; (C) ^{18}F-Flumazenil PET: focal defect of tracer uptake at the right hippocampus.

Neurobiology of Disease 109 (2018) 76–87

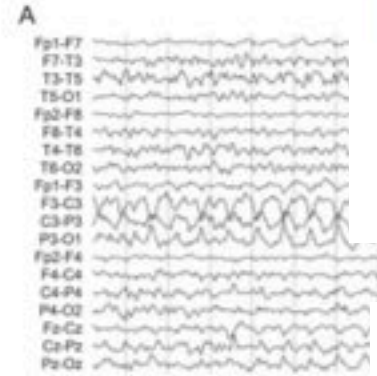
A distinct microRNA expression profile is associated with α[^{11}C]-methyl-L-tryptophan (AMT) PET uptake in epileptogenic cortical tubers resected from patients with tuberous sclerosis complex

Shruti Bagla[a], Daniela Cukovic[a], Eishi Asano[a], Sandeep Sood[e], Aimee Luat[a], Harry T. Chugani[b], Diane C. Chugani[c,d], A

Clinical Applications of Simultaneous PET/MR Imaging Using (*R*)-[^{11}C]-Verapamil with Cyclosporin A: Preliminary Results on a Surrogate Marker of Drug-Resistant Epilepsy

J.-W. Shin, K. Chu, S.A. Shin, K.-H. Jung, S.-T. Lee, Y.-S. Lee, J. Moon, D.Y. Lee, J.S. Lee, D.S. Lee and S.K. Lee

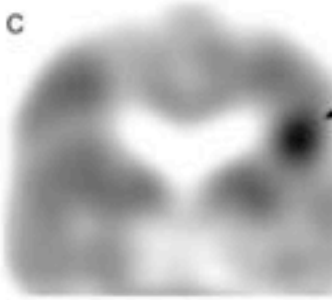
American Journal of Neuroradiology April 2016, 37 (4) 600-606; DOI: https://doi.org/10.3174/ajnr.A4566



ACS Chemical Neuroscience

Research Article

pubs.acs.org/chemneuro



Scalp ictal EEG (A), FDG (B), and AMT (C) PET scans of rhythmic sharply contoured slow-wave activity arising showed multifocal and bilateral hypometabolic region inferior lateral parietal region (arrow) can be seen. Th with subdural electrodes are shown in D and E. (B) Glucose hypometabolic areas are indicated by violet areas in the left inferior parietal and frontal regions. (E) Increased AMT uptake (indicated in red) in the left inferior parietal region (arrow). Ictal subdural EEG recording showed seizure onset (white electrodes) originating from the left primary sensory face area. The child was seizure-free after surgery (follow-up 4 years). AMT = α-[^{11}C]-methyl-L-tryptophan; FDG = 2-deoxy-2-[^{18}F]fluoro-D-glucose.

Synthesis and Evaluation of New Fluorine-18 Labeled Verapamil Analogs To Investigate the Function of P-Glycoprotein in the Blood–Brain Barrier

Renske M. Raaphorst,[*,†] Gert Luurtsema,[‡] Robert C. Schuit,[†] Esther J. M. Kooijman,[†] Philip H. Elsinga,[‡] Adriaan A. Lammertsma,[†] and Albert D. Windhorst[†]

[†]Department of Radiology & Nuclear Medicine, VU University Medical Center, 1081 HV Amsterdam, The Netherlands

[‡]Department of Nuclear Medicine and Molecular Imaging, University Medical Center Groningen, University of Groningen, 9712 CP Groningen, The Netherlands

Schizophrénie

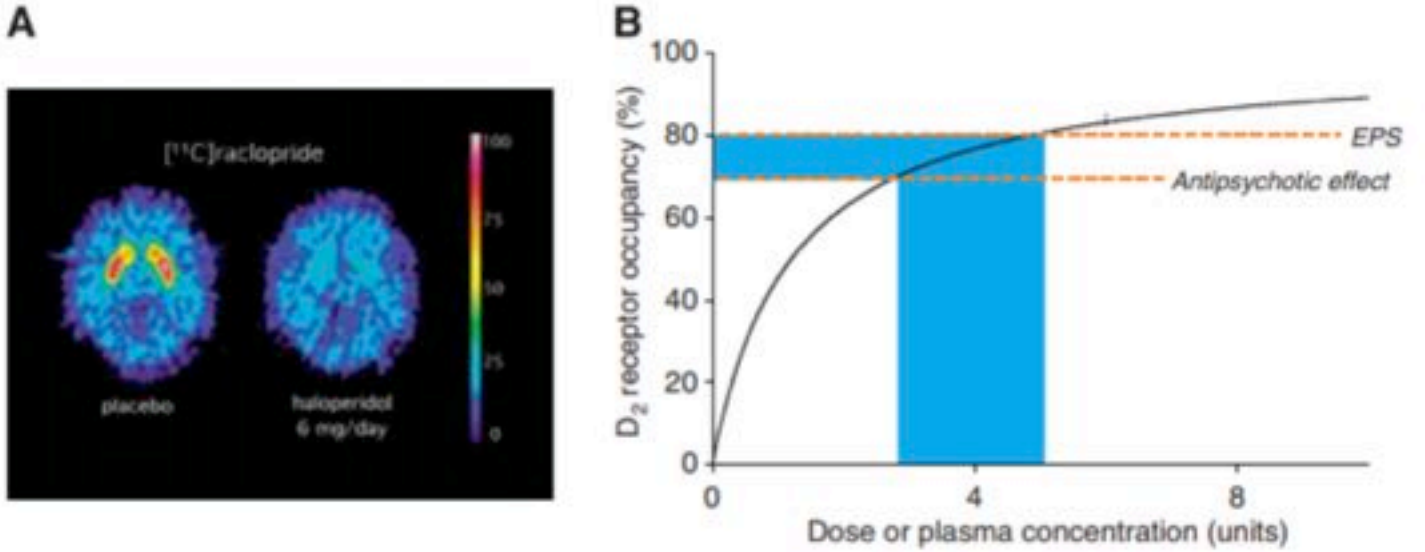


Figure 4 (**A**) [^{11}C]raclopride positron emission tomography (PET) images through the caudate/putamen level of a schizophrenic patient treated with placebo (left) and haloperidol (right) as described in Farde *et al* (1992). (**B**) The suggested distinct thresholds for antipsychotic effects and extrapyramidal syndromes (EPSs) as induced by classical antipsychotic drugs. Owing to the hyperbolic relationship between occupancy of the D_2 receptor and dose of antipsychotic drug (or plasma concentration) there is a rather narrow interval for optimal therapeutic treatment. Figure modified from Farde (1996).

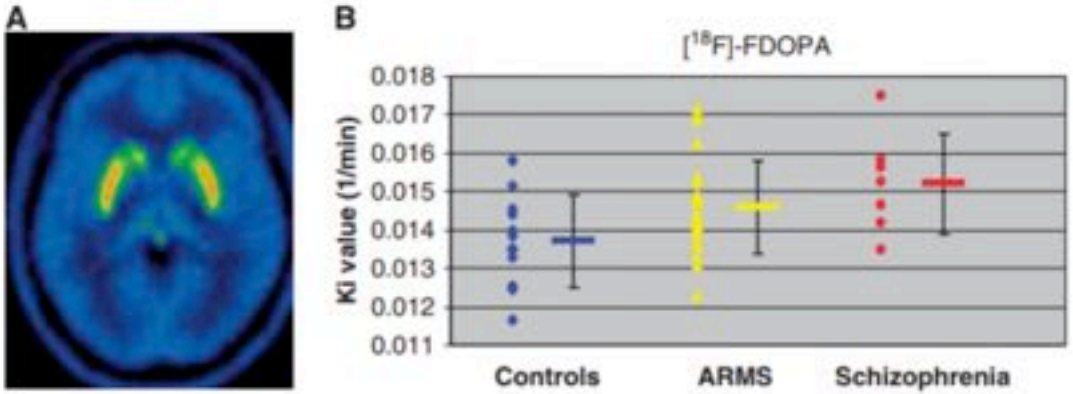


Figure 5 (**A**) Straital [^{18}F]16-fluoro-L-DOPA ([^{18}F]F-DOPA) summation image. (**B**) Individual and group striatal [^{18}F]F-DOPA Ki values (influx rate constants) for normal controls, subjects with At-Risk Mental Status (ARMS) and those with schizophrenia, showing significantly higher ($P < 0.05$) Ki values in schizophrenia patients compared with controls. (**C**) Positive correlation between total Comprehensive Assessment of At-Risk Mental States (CAARMS) score (higher score indicates greater severity of prodromal symptoms) and Ki values (Howes *et al*, 2009).

Imagerie de l'addiction



Imaging Neurotransmitter Release by Drugs of Abuse

Diana Martinez and Rajesh Narendran

mutant has become the preferred method for imaging presynaptic dopamine transmission, and this method has been used in studies of addiction. The results of these studies suggest that cocaine and alcohol addiction are associated with a loss of dopamine transmission, and a number of studies show that this loss correlates with severity of disease.

Dépression et anxiété

- Dépressifs majeurs ont peu de recepteurs 5HTa1 et une faible concentration en récepteurs 5HTa2 (thérapeutique)
- Avidité aux enzymes catabolique MAO-A (11C-harmin) au cortex préfrontal et cingulaire antérieur chez les patients à risque de récidive dépressive est corrélée à une tendance à la dépression post partum sevrage tabac (Bachar 2011).
- elevation en transporteurs sérotoninergiques dans les régions de modulation affective en hiver plus qu'en été (Kalbitzer 2010)

Tumeurs cérébrales

- FDG au débuts
- Acides aminés (11C-methio, 11C-thyro): synthèse protéïque (meilleur S/B) ou mieux FET
- FLT: thymidine profilération cellulaire
- F misonidazole: imagerie de l'hypoxie…

Développement pharmaceutique, amélioration des connaissances sur le cerveau…

Démences

Tc-99m HMPAO SPECT in the Differential Diagnosis of the Dementias With Histopathologic Confirmation

Frederick J. Bonte, MD,† Thomas S. Harris, MS,*† Linda S. Hynan, PhD,‡ Eileen H. Bigio, MD‖§ and Charles L. White III, MD§*

(*Clin Nucl Med* 2006;31: 376–378)

TABLE 2. For the Diagnosis of Alzheimer Disease With and Without Lewy Bodies

	95% Confidence Interval	
Proportion	**Lower Limit**	**Upper Limit**
Sensitivity: 26/30 = 86.7%	68.4%	95.6%
Specificity: 17/19 = 89.5%	65.5%	98.2%
Positive predictive value: 26/28 = 92.9%	75.0%	98.8%
Negative predictive value: 17/21 = 81.0%	57.4%	93.7%
Accuracy: 43/49 = 87.8%	74.5%	94.9%

TABLE 3. Diagnosis of Alzheimer Disease vs. Histopathology

Series	Present	Jobst et al[7]	Silverman et al[8]	Hoffman et al[9]
Total studied	49	104	70	22
Modality	SPECT	SPECT	PET	PET
Sensitivity (CI)	86.7% (68.4–95.6%)	89%	96%	87.5%
Specificity (CI)	89.5% (65.5–98.2%)	80%		66.7%
PPV (CI)	92.9% (75.0–98.8%)			87.5%
NPV (CI)	81.0% (57.4–93.7%)			66.7%
Accuracy (CI)	87.8% (74.5–94.9%)	83%	87.1% (+/− 7.8%)	81.8%

CI indicates confidence interval; NPV, negative predictive value; PPV, positive predictive value.

Effectiveness and Safety of ^{18}F-FDG PET in the Evaluation of Dementia: A Review of the Recent Literature

Nicolaas I. Bohnen[1–3], David S.W. Djang[4], Karl Herholz[5], Yoshimi Anzai[6,7], and Satoshi Minoshima[6]

J Nucl Med 2012; 53:59–71
DOI: 10.2967/jnumed.111.096578

Association Nationale de Médecine Nucléaire Libérale

Reference and AAN level	Diagnostic standard	Study type	Subjects	Major findings
Silverman et al., 2001 (*42*), AAN level II	Autopsy confirmation and clinical follow-up	Multicenter retrospective analysis based on postmortem diagnosis	AD (n = 97); non-AD (n = 41), such as progressive supranuclear palsy, Parkinson disease, cerebrovascular disease, or mixed	AD was identified in 85/89 (sensitivity, 96%) AD-only cases and 6/8 AD-plus cases (overall sensitivity, 94%). Absence of AD was confirmed in 30/41 cases (specificity, 73%), including 23 with other neurodegenerative dementias. Absence of neurodegenerative disease was confirmed in 14/18 cases (specificity, 78%). Negative PET scan indicated that pathologic progression of cognitive impairment during mean 3-y follow-up was unlikely.
Jagust et al., 2007 (*39*), AAN level II	Autopsy confirmation	Retrospective study with 4-y clinical follow-up and 5 y until death and autopsy	Forty-four subjects with dementia, cognitive impairment, or normal cognitive functions; postmortem diagnosis included AD (n = 20), FTD, DLB, mixed, and vascular dementia	For diagnosing AD, accuracy of ^{18}F-FDG PET (sensitivity, 84%; specificity, 74%) was better than that of initial clinical evaluation (sensitivity, 76%; specificity, 58%). ^{18}F-FDG PET (76%) also had better NPV than did initial clinical evaluation (65%).
Minoshima et al., 2001 (*41*), AAN level II	Autopsy confirmation and clinical follow-up	Retrospective ^{18}F-FDG PET analysis based on postmortem diagnosis, and retrospective ^{18}F-FDG PET diagnosis based on clinical follow-up	AD (n = 10); autopsy-confirmed DLB (n = 11); additional 53 patients with clinically probable diagnosis of AD (n = 40) or DLB (n = 13) based on follow-up evaluation	^{18}F-FDG PET can distinguish AD from DLB with 90% sensitivity and 80% specificity.
Foster et al., 2007 (*16*), AAN level II	Autopsy confirmation	Retrospective consensus study of 6 dementia experts reviewing clinical history and ^{18}F-FDG PET studies	AD (n = 31); FTD (n = 14); controls (n = 33)	^{18}F-FDG PET is significantly more accurate in distinguishing FTD from AD than clinical methods. ^{18}F-FDG PET adds important information that appropriately increases diagnostic confidence, even among experienced dementia specialists. Mean interrater κ was 0.31–0.42 for clinical information and 0.73–0.78 for ^{18}F-FDG PET. For AD diagnosis compared with FTD, sensitivity was 96.7% and specificity was 85.7%.

CONFIRMATION ANAPATH

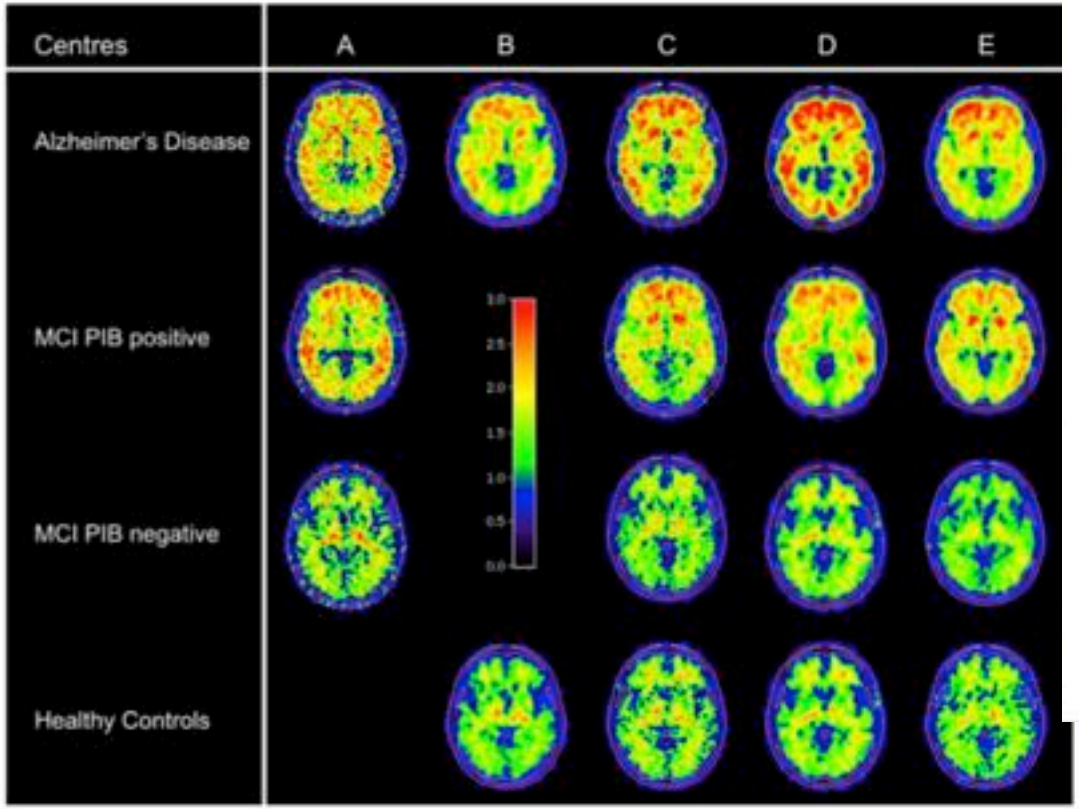
FDG

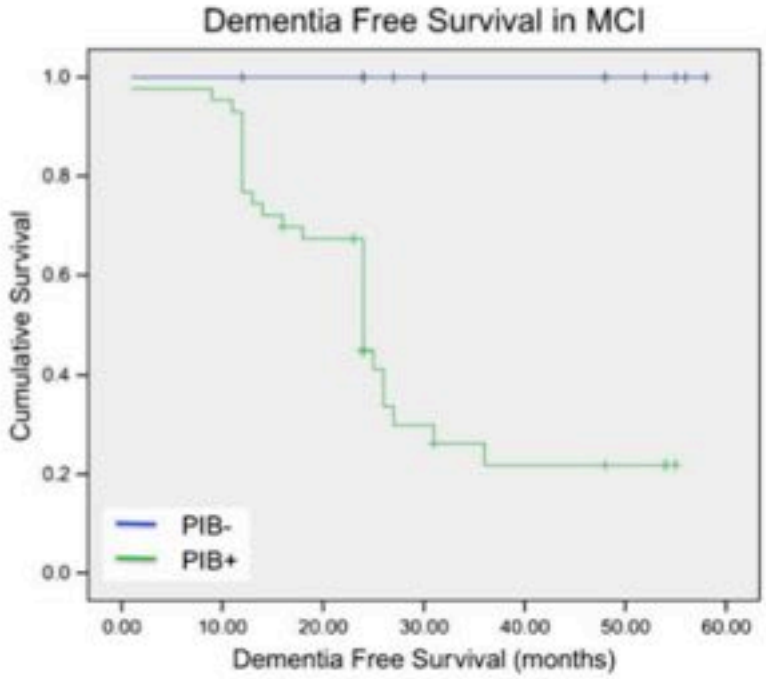
CLINIQUE

Eur J Nucl Med Mol Imaging (2013) 40:104–114
DOI 10.1007/s00259-012-2237-2

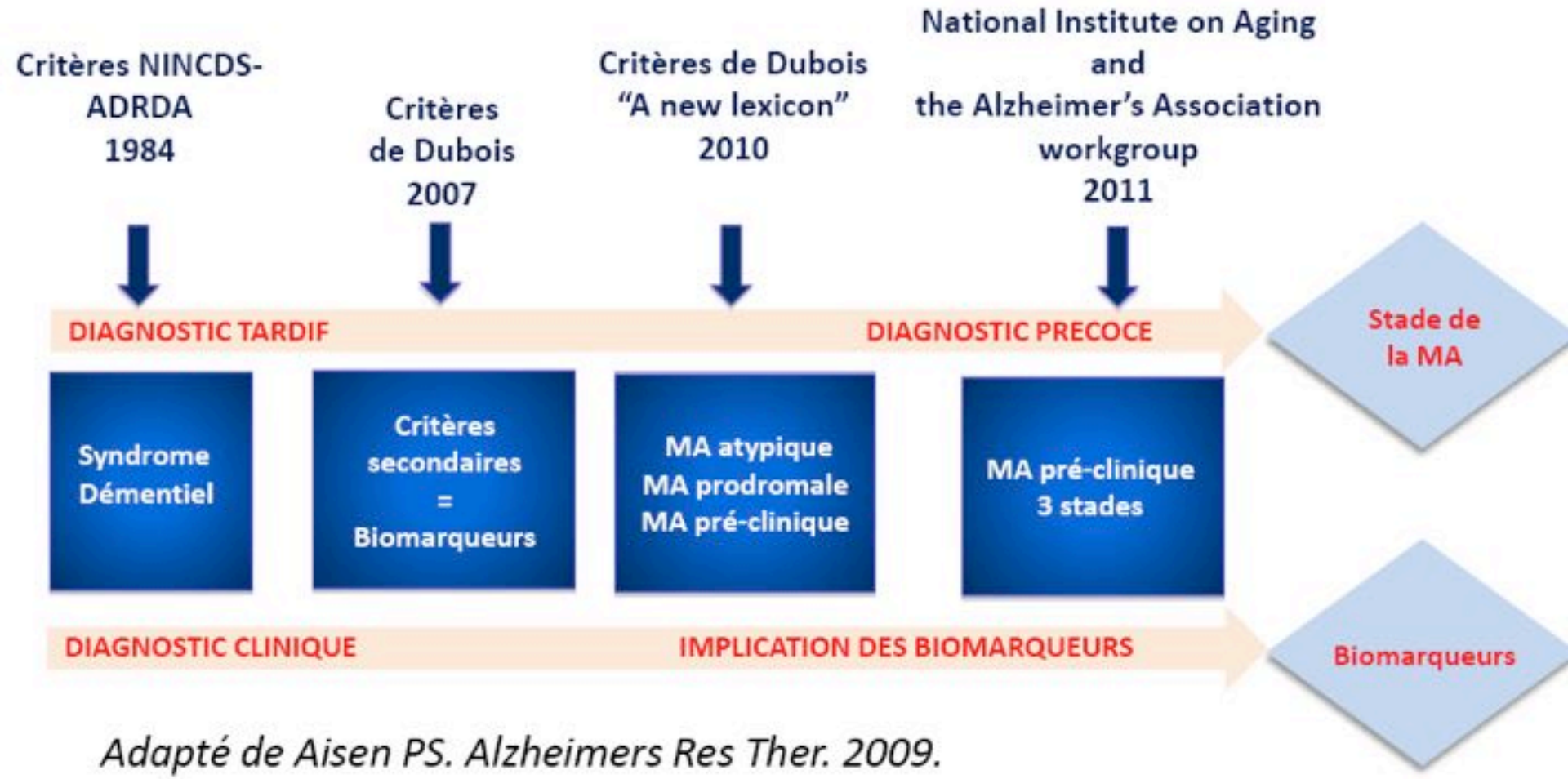
ORIGINAL ARTICLE

A European multicentre PET study of fibrillar amyloid in Alzheimer's disease





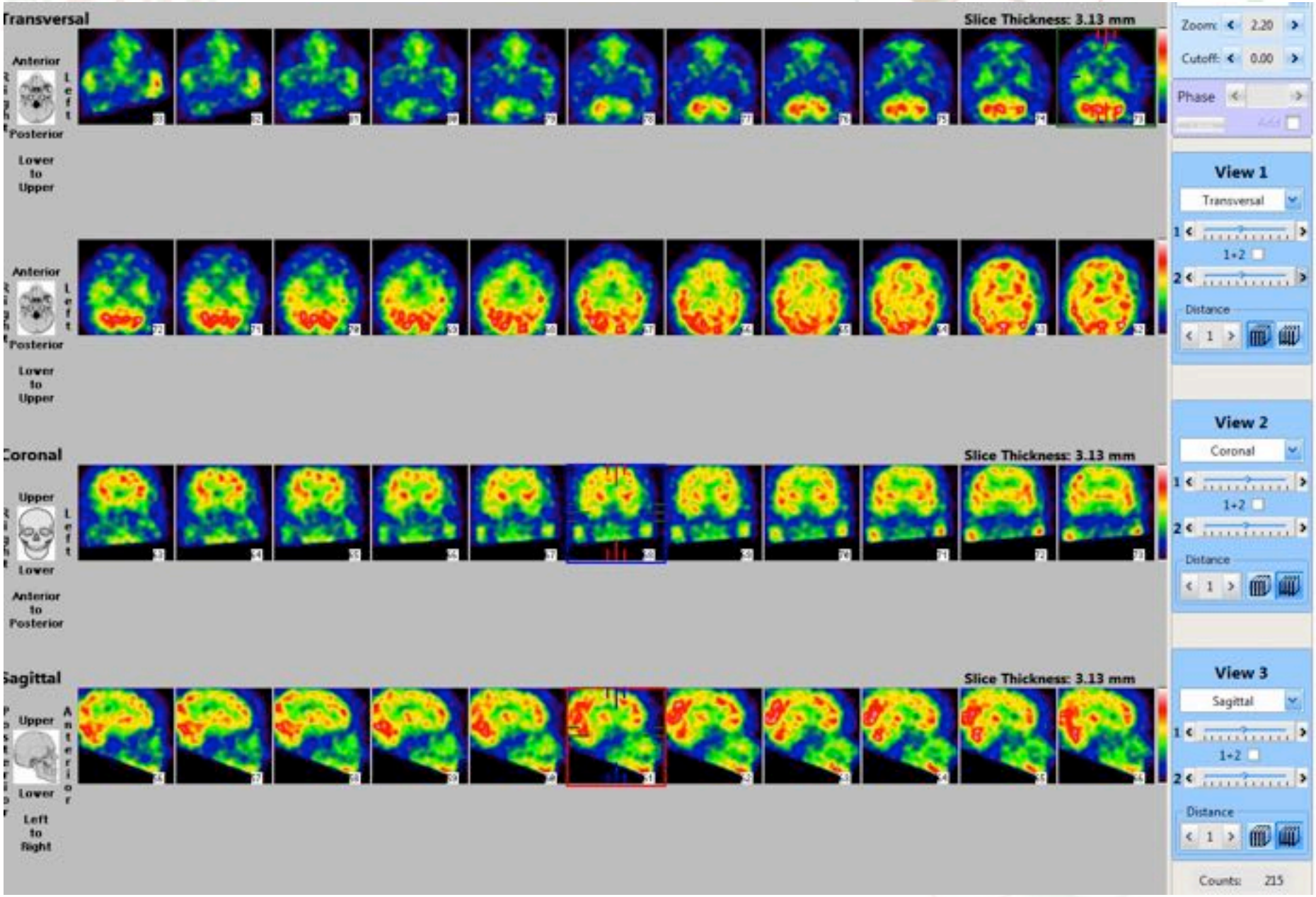
Diagnostic de la MA: évolution des critères de 1984 à 2011

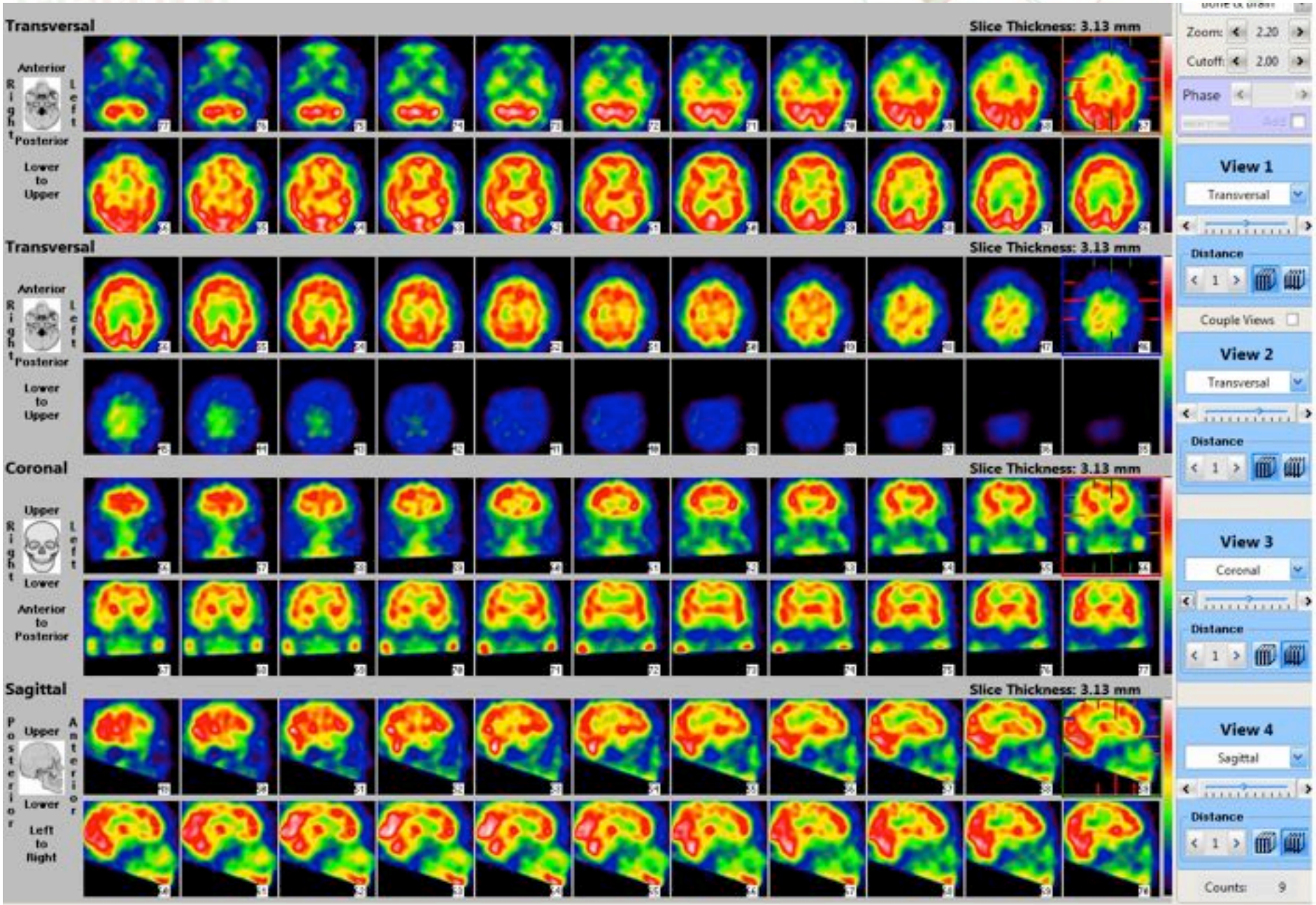


Adapté de Aisen PS. Alzheimers Res Ther. 2009.

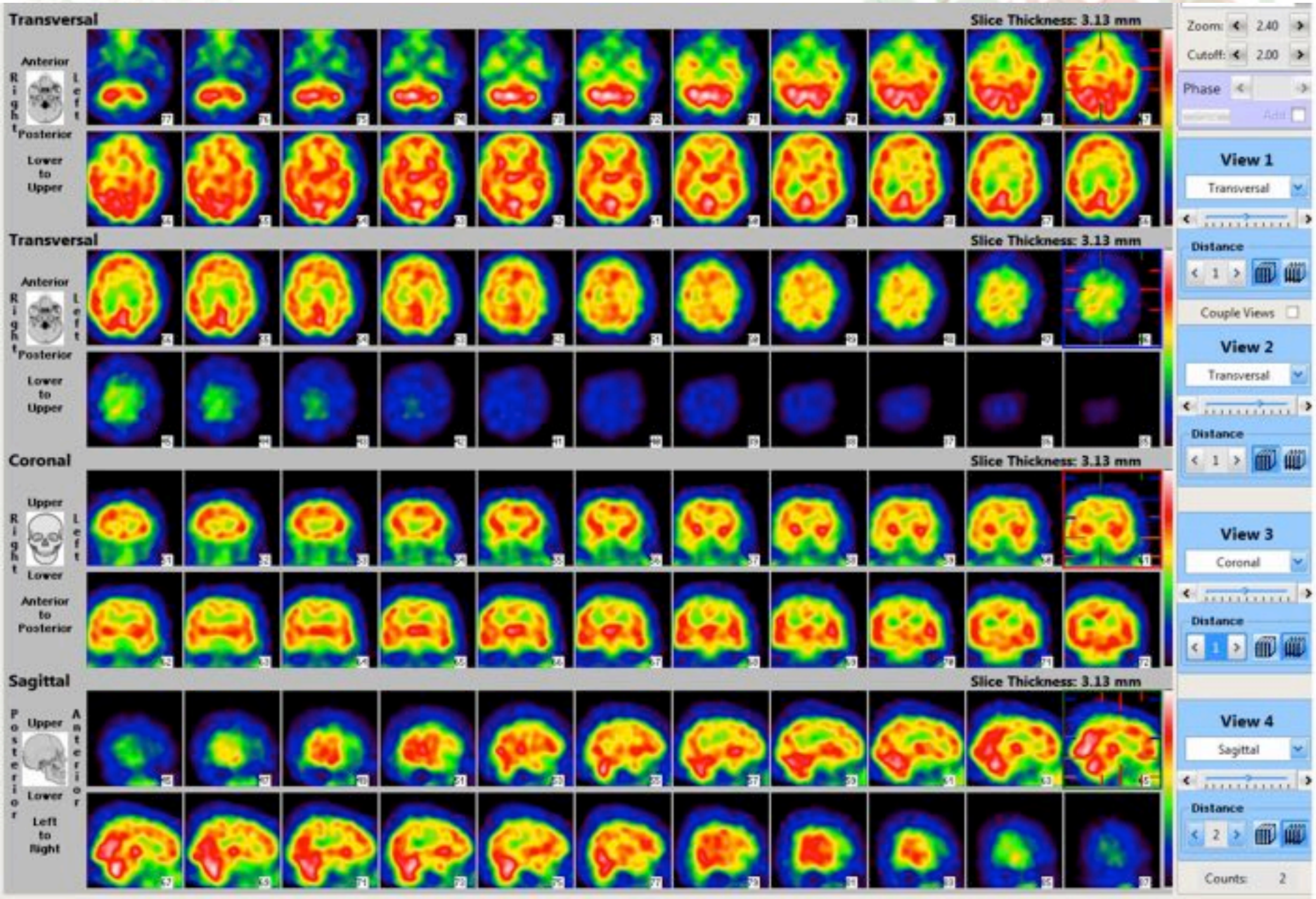
pourquoi faire la neurologie nucléaire à Sidi Bel Abbes

- Domaine passionnant
- Continuer le travail entamé au CHU Tlemcen
- Répondre à un besoin réel
- Augmentation de l'incidence de la maladie démentielle
- Examens facilement réalisables peu couteux
- Outils précis
- Rôle de plus en plus important des biomarqueurs d'imagerie dans les cas de démence probable.

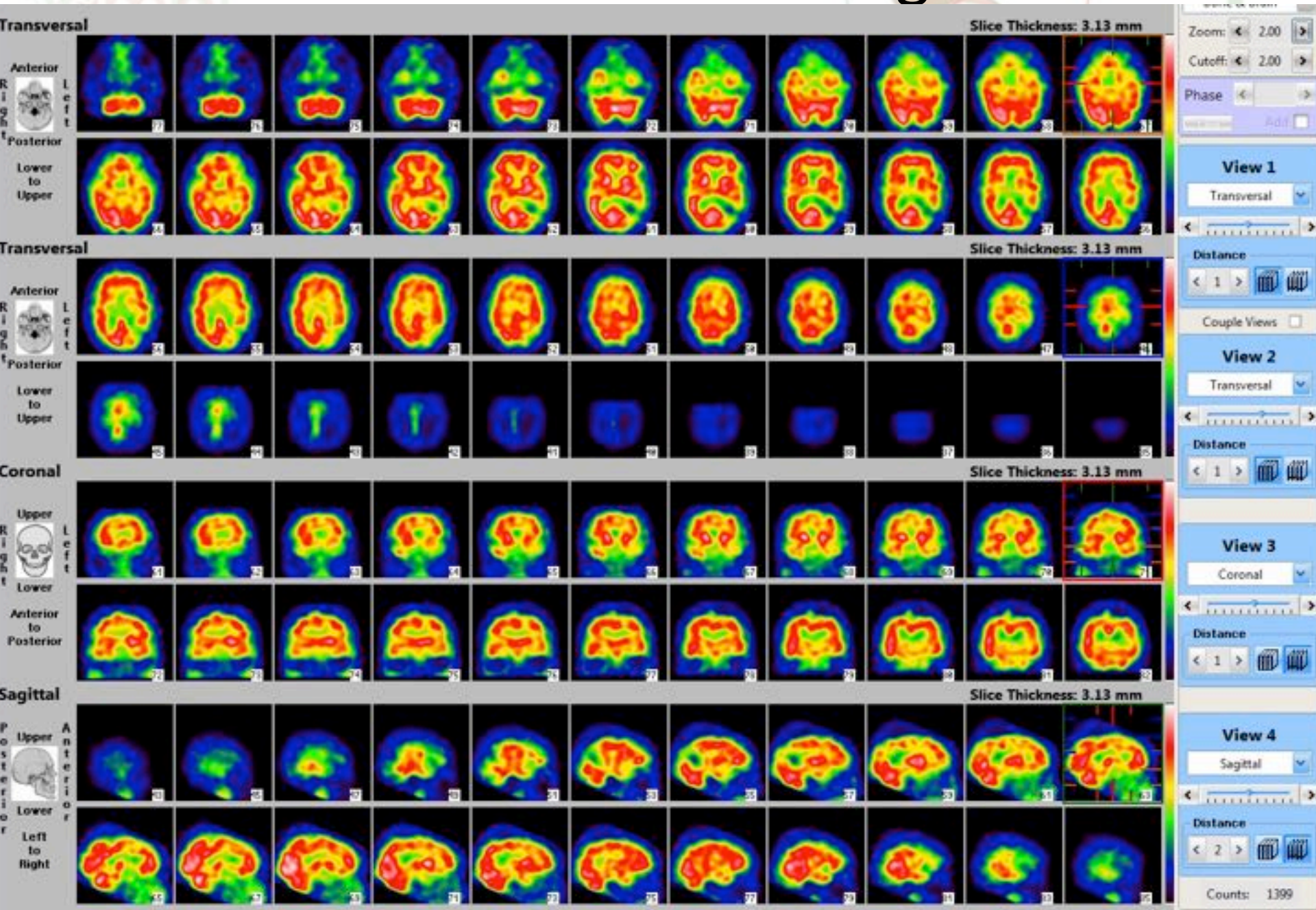

Transversal
Slice Thickness: 3.13 mm
Anterior
Left
Posterior
Lower to Upper
Anterior
Left
Posterior
Lower to Upper
Coronal
Slice Thickness: 3.13 mm
Upper
Left
Lower
Anterior to Posterior
Sagittal
Slice Thickness: 3.13 mm
Upper
Anterior
Lower
Left to Right
Zoom: 2.20
Cutoff: 0.00
Phase
View 1
Transversal
1+2
Distance
1
View 2
Coronal
1+2
Distance
1
View 3
Sagittal
1+2
Distance
1
Counts: 215


Transversal
Slice Thickness: 3.13 mm
Anterior
Right
Left
Posterior
Lower to Upper
Transversal
Slice Thickness: 3.13 mm
Anterior
Right
Left
Posterior
Lower to Upper
Coronal
Slice Thickness: 3.13 mm
Upper
Right
Left
Lower
Anterior to Posterior
Sagittal
Slice Thickness: 3.13 mm
Posterior
Upper
Anterior
Lower
Left to Right
Zoom: 2.20
Cutoff: 2.00
Phase
View 1
Transversal
Distance
Couple Views
View 2
Transversal
Distance
View 3
Coronal
Distance
View 4
Sagittal
Distance
Counts: 9

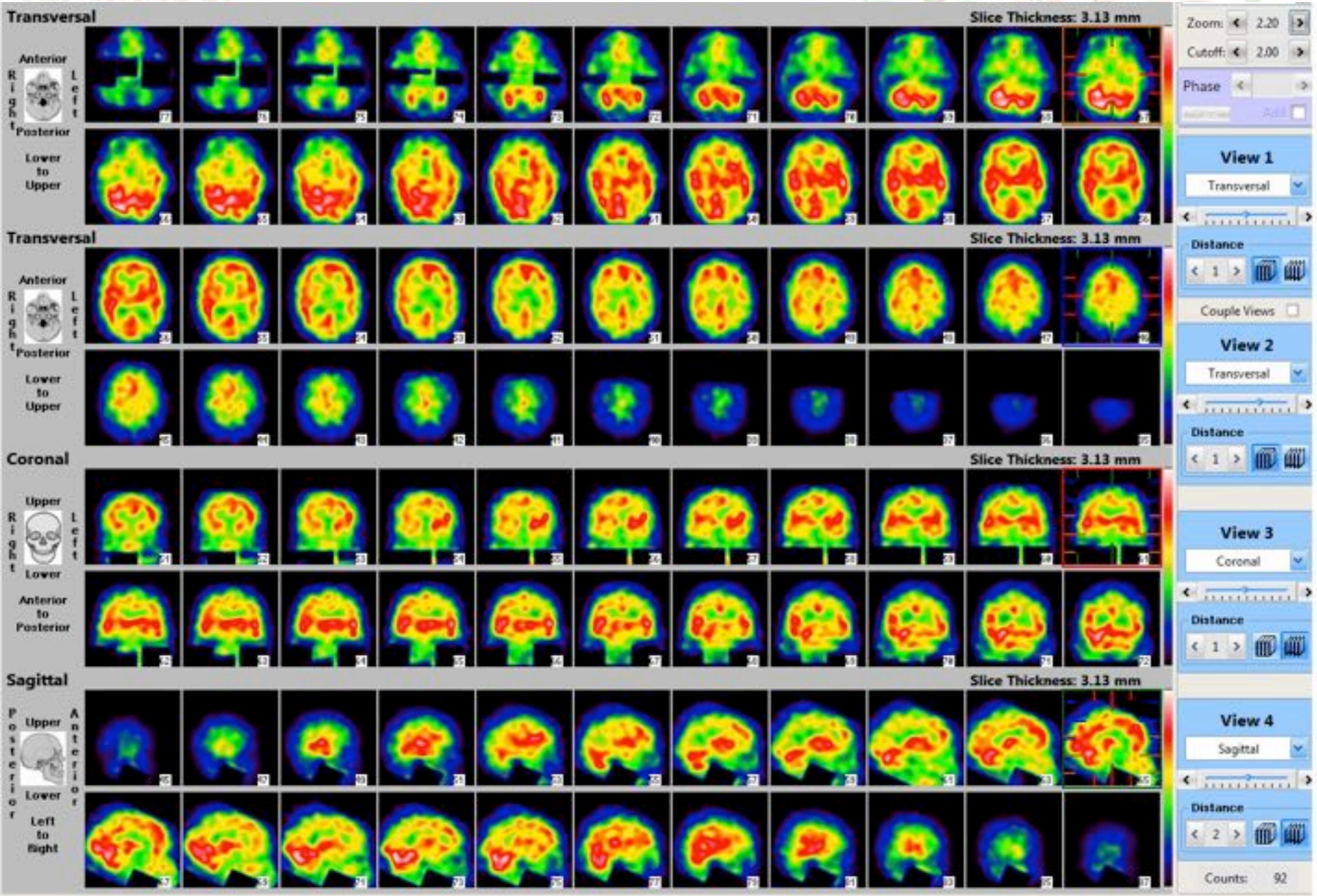
EXAMEN NORMAL



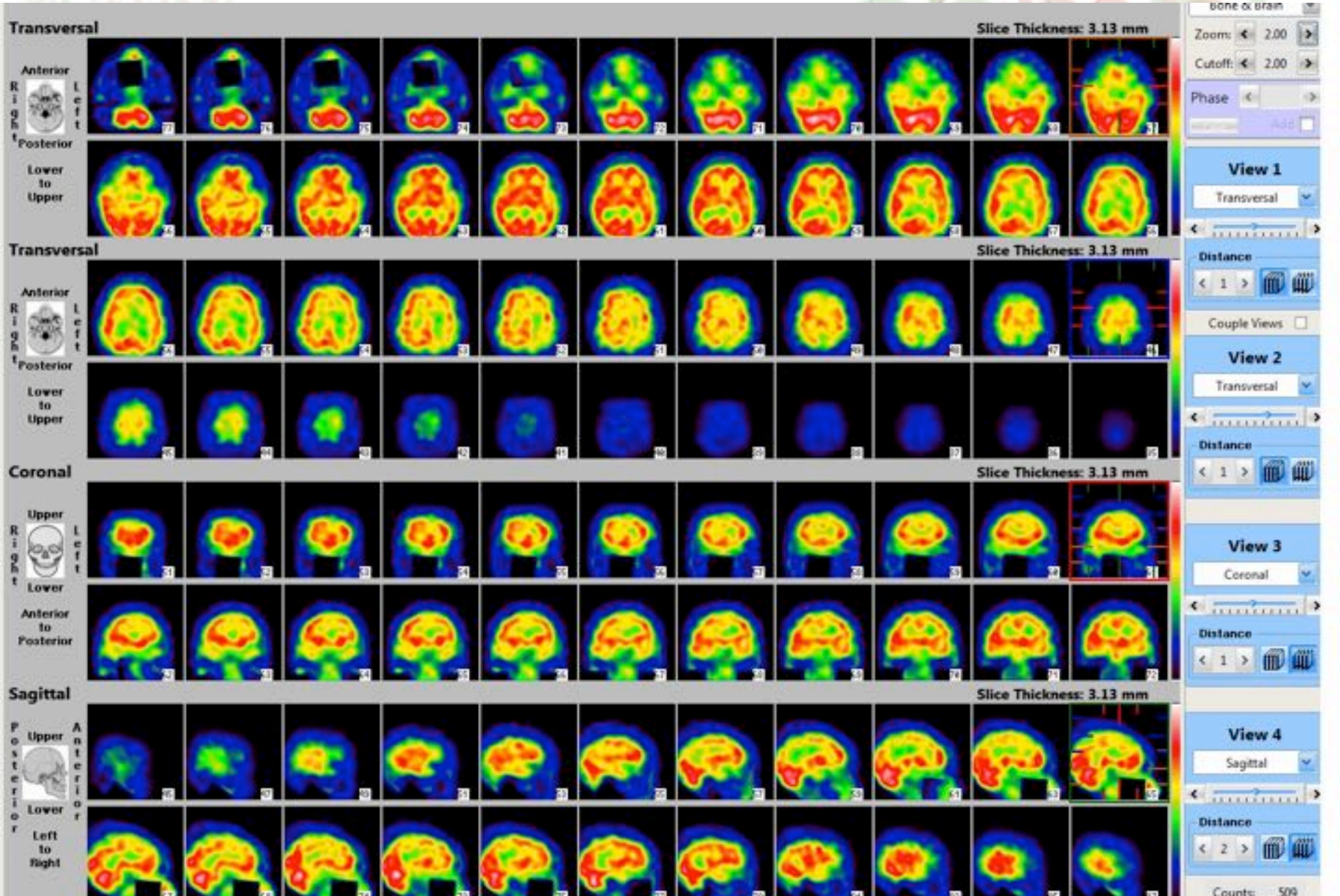
Démence mixte vasc et degenerative



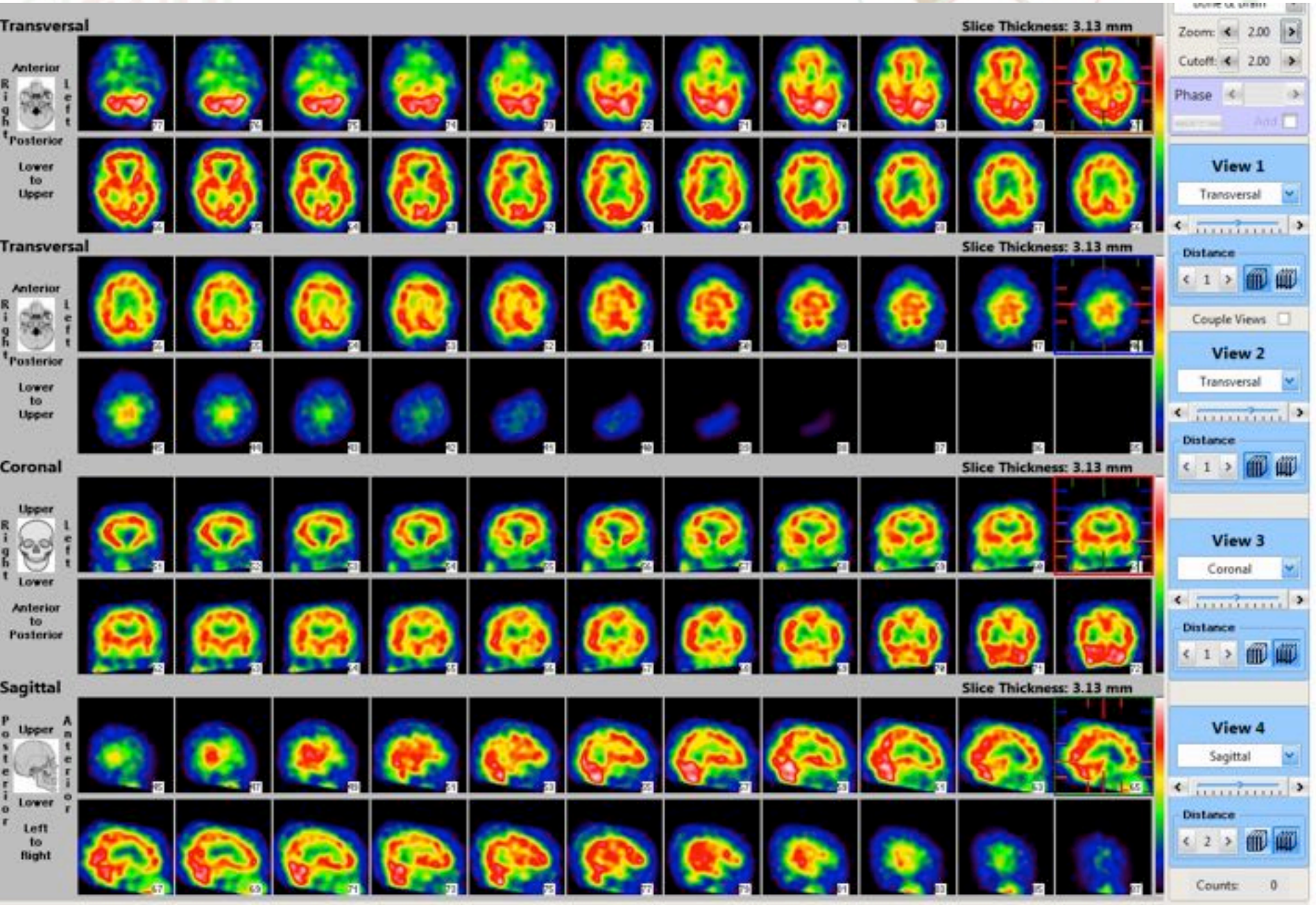
L.N. 70 ans troubles mnésiques



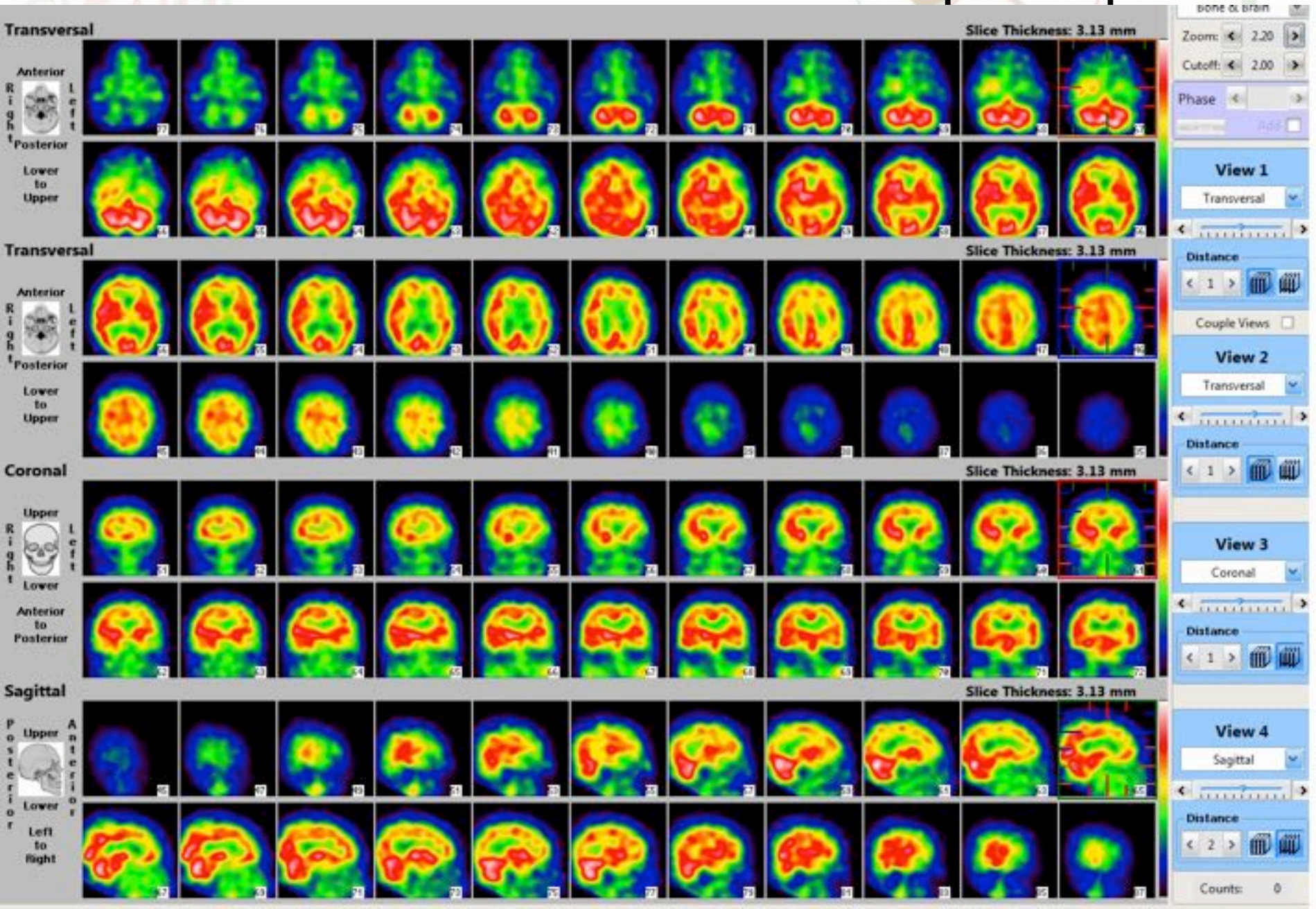
A.M. homme. Droitier. S.extraP. MMSE 27



B.M femme 74 ans. Troubles phasiques



L.A.Z. femme 68 ans. Troubles phasiques













و شكرا



